Microfluidic gradient device for studying mesothelial cell migration and the effect of chronic carbon nanotube exposure

2015 J. Micromech. Microeng. 25 075010

(http://iopscience.iop.org/0960-1317/25/7/075010)

IOP Publishing Journal of Micromechanics and Microengineering
J. Micromech. Microeng. **25** (2015) 075010 (12pp) doi:10.1088/0960-1317/25/7/075010

Microfluidic gradient device for studying mesothelial cell migration and the effect of chronic carbon nanotube exposure

Hanyuan Zhang[1], Warangkana Lohcharoenkal[2], Jianbo Sun[1], Xiang Li[1], Liying Wang[3], Nianqiang Wu[4], Yon Rojanasakul[2] and Yuxin Liu[1]

[1] Lane Department of Computer Science and Electrical Engineering, West Virginia University, Morgantown, WV 26506, USA
[2] Department of Basic Pharmaceutical Sciences, West Virginia University, Morgantown, WV 26506, USA
[3] Pathology and Physiology Research Branch, National Institute for Occupational Safety and Health, Morgantown, WV 26505, USA
[4] Department of Mechanical and Aerospace Engineering, West Virginia University, Morgantown, WV 26506, USA

E-mail: yuxin.liu@mail.wvu.edu

Received 21 February 2015, revised 15 April 2015
Accepted for publication 27 April 2015
Published 3 June 2015

Abstract

Cell migration is one of the crucial steps in many physiological and pathological processes, including cancer development. Our recent studies have shown that carbon nanotubes (CNTs), similarly to asbestos, can induce accelerated cell growth and invasiveness that contribute to their mesothelioma pathogenicity. Malignant mesothelioma is a very aggressive tumor that develops from cells of the mesothelium, and is most commonly caused by exposure to asbestos. CNTs have a similar structure and mode of exposure to asbestos. This has raised a concern regarding the potential carcinogenicity of CNTs, especially in the pleural area which is a key target for asbestos-related diseases. In this paper, a static microfluidic gradient device was applied to study the migration of human pleural mesothelial cells which had been through a long-term exposure (4 months) to subcytotoxic concentration ($0.02\,\mu g\,cm^{-2}$) of single-walled CNTs (SWCNTs). Multiple migration signatures of these cells were investigated using the microfluidic gradient device for the first time. During the migration study, we observed that cell morphologies changed from flattened shapes to spindle shapes prior to their migration after their sensing of the chemical gradient. The migration of chronically SWCNT-exposed mesothelial cells was evaluated under different fetal bovine serum (FBS) concentration gradients, and the migration speeds and number of migrating cells were extracted and compared. The results showed that chronically SWCNT-exposed mesothelial cells are more sensitive to the gradient compared to non-SWCNT-exposed cells. The method described here allows simultaneous detection of cell morphology and migration under chemical gradient conditions, and also allows for real-time monitoring of cell motility that resembles *in vivo* cell migration. This platform would be much needed for supporting the development of more physiologically relevant cell models for better assessment and characterization of the mesothelioma hazard posed by nanomaterials.

Keywords: microfluidics, static gradient device, cell migration, nanomaterial effects, human pleural mesothelial cells

S Online supplementary data available from stacks.iop.org/JMM/25/075010/mmedia

(Some figures may appear in colour only in the online journal)

1. Introduction

1.1. Microfluidic gradient devices for cell migration study

Cell migration is known to be a crucial step in many physiological events including embryogenesis, morphogenesis, neurogenesis angiogenesis, wound healing, and inflammation, and is also implicated in the pathophysiology of many diseases including cancers (von der Mark *et al* 1999, Cho and Klemke 2000). Enhanced cell migration is a key feature of aggressive tumors and has been used as a predictive indicator of tumor metastasis (Kaufman and Flores 2011).

To date, *in vitro* cell migration assays employ conventional methods such as under-agarose assay (Heit and Kubes 2003), Boyden chambers (Boyden 1962), Dunn chambers (Zicha *et al* 1991), Zigmond chambers (Zigmond 1977), and micropipette-based assay (Servant *et al* 1999). However, these assays are limited in providing reliably controlled chemical gradients and are lacking in analysis of migration speed and cell morphological changes as well as real-time monitoring of cell migration. These disadvantages can be overcome by using microfluidic devices, which have been applied to study cell migration (Frevert *et al* 2006, Liu *et al* 2008, Kim *et al* 2010).

Microfluidic platforms for gradient generation can be classified into five categories: laminar flow gradients, static gradient, 3D gradients, 1D gradients, and immobilized gradients. Comprehensive reviews for microfluidic gradient platforms were reported previously (Kim *et al* 2010, Berthier and Beebe 2014). For studies of cell migration on 2D substrates under the effects of soluble chemoattractant gradients, laminar flow-based platforms, static gradient devices, or 1D gradient devices are commonly chosen. For a laminar flow-based microfluidic gradient device, the gradient was generated by diffusion with a progressive mix of compounds from different concentrations of fluid streams, and the gradient was transverse to the direction of the flow. This type of device offers precisely controlled stable gradients over time. However, the shear stress induced by the constant flow can affect cellular migration as well as induce undesired signaling events (Berthier and Beebe 2014). The static gradient (Diao *et al* 2006, Berthier *et al* 2010) and 1D gradient platforms (Boneschansker *et al* 2014, Irimia 2014) have been developed to reduce interference due to shear stresses caused by continuous flows. Using a high fluidic resistance as an integrated section, such as an integrated high resistant porous membrane (Diao *et al* 2006), has been shown to effectively minimize or prevent convective flows and generate gradient based on static diffusion of chemoattractants.

1.2. Human pleural mesothelial cells and long-term exposure to SWCNTs

Mesothelial cells are specialized cells forming a protective non-adhesive surface lining the serosal cavities and internal organs (Mutsaers 2002), and have a variety of functions including enzyme regulation and production (Martin *et al* 2000), antigen presentation (Valle *et al* 1995), and fluid and cell transportation. Malignant mesothelioma, a rare form of cancer developed from mesothelial cells, is a very aggressive tumor with low survival rate and no effective treatment. The most common anatomical site for mesothelioma is the pleura (the outer lining of the lungs and internal chest wall), but it can also arise in the peritoneum (the lining of the abdominal cavity) or the pericardium (the sac that surrounds the heart) (Kaufman and Flores 2011). About 70% of all diagnosed malignant mesothelioma cases are pleural mesothelioma (Bridda *et al* 2007) and chronic exposure to asbestos fibers is recognized as the major cause (Carbone *et al* 2002).

CNTs are high-aspect-ratio cylinders of one (single-walled) or several coaxial (multi-walled) graphite layer(s) with nanoscale diameters and microscale lengths (Foldvari and Bagonluri 2008, Shvedova *et al* 2009). With structural similarity as well as a similar exposure mode to asbestos, concerns about the potential carcinogenicity of CNTs have been raised, especially in the pleural space, which is a key target tissue for asbestos-related diseases (Lohcharoenkal *et al* 2013). *In vivo* studies have shown that CNTs have been found in the alveolar epithelium, the mucous lining layer, the air spaces and interstitium, and the pulmonary venule (Mercer *et al* 2008, 2011, Wang *et al* 2010, 2013). They were biopersistent with low clearance rate, can cause inflammation, fibrosis, and granuloma formation (Lam *et al* 2004, Muller *et al* 2005, Chou *et al* 2008), and have the potential to further induce mesothelioma (Elgrabli *et al* 2008). We have previously developed an *in vitro* chronic exposure model to mimic CNT-induced malignant transformation and demonstrated the induction of cancer phenotypes of pleural mesothelial cells by CNTs that may contribute to their mesothelioma pathogenicity (Wang *et al* 2013).

Our earlier experiment indicated that shear stresses induced by the constant flow greatly affected mesothelial cells' attachment in the laminar flow-based gradient device. In this paper, we presented a microfluidic static gradient device to satisfy the specific needs for studying the migration of human pleural mesothelial cells chronically exposed to subcytotoxic concentration of CNTs, including substrate coating, static gradient generation, extended experimental duration up to 24 h for real-time monitoring cell migration, and analysis of multiple migration signatures. To our best knowledge, there is no report on utilizing microfluidic gradient devices for studying nanomaterials' effects on cell migration. It is important to develop approaches as well as cell models for better assessment and characterization of the mesothelioma hazard posed by nanomaterials.

2. Materials and methods

2.1. Device design and fabrication

A microfluidic device was designed and fabricated for static gradient generation and live cell imaging. The device consisted of a cell-seeding chamber, five migration channels and a cell-receiving chamber as shown in figure 1. Two devices were fabricated on a glass slide together. For each experiment, under the same FBS concentration gradient, one device was used for observing SWCNT-exposed cells, and the other

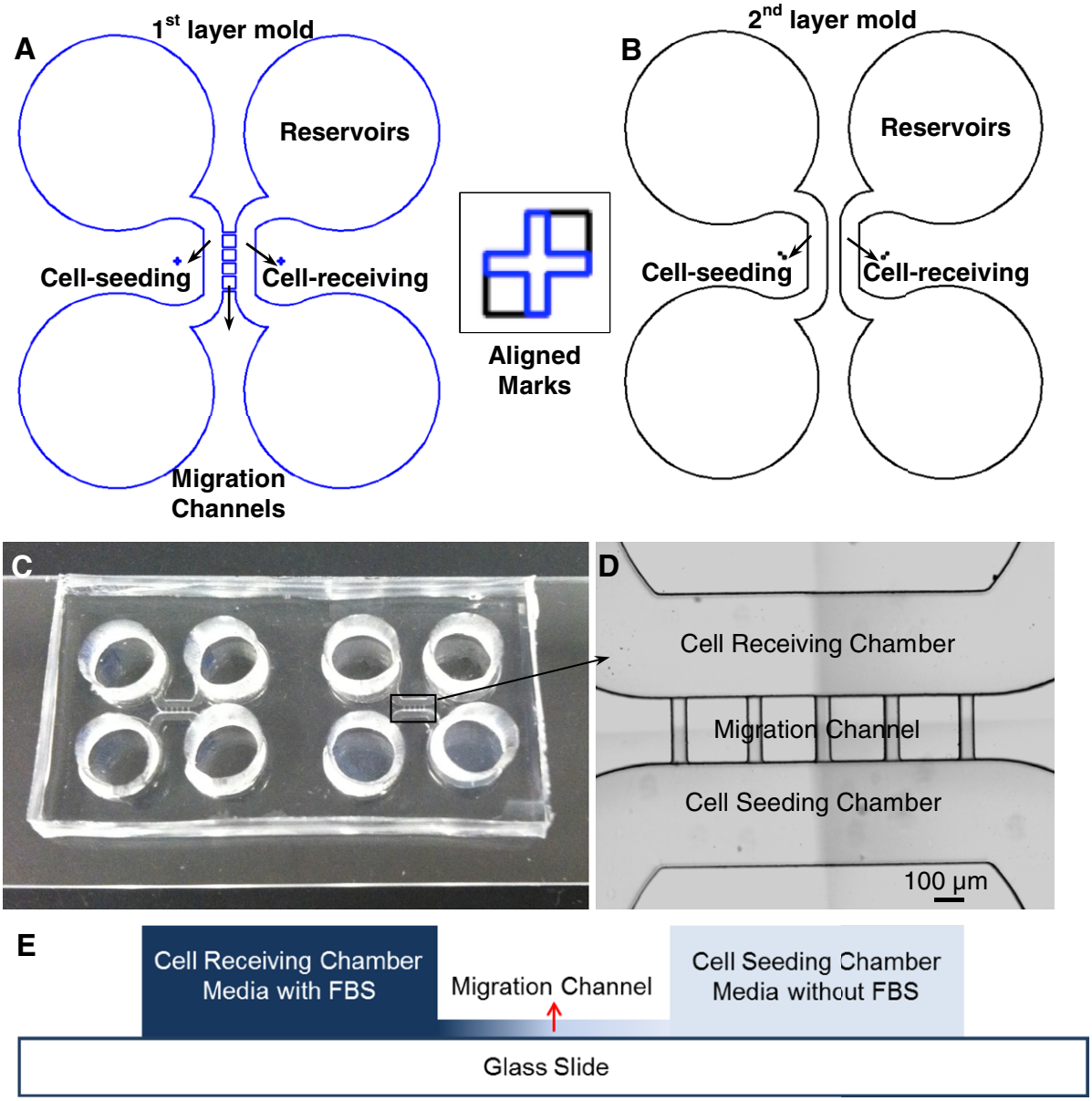

Figure 1. Schematic diagram of the molds for fabrication of the gradient device. (A) The first shallow mold layer (16 μm) to define four reservoirs, cell-seeding/receiving chambers, and five migration channels. (B) The second mold layer to define four reservoirs and cell-seeding/receiving chambers. The square box shows the alignment marks on both layers. (C) Two devices fabricated and bonded on one glass slide; the size of the two devices together is 2 × 4 cm. (D) Image shows the cell-receiving chamber, the migration channels, and the cell-seeding chamber, respectively; the scale bar is 100 μm. (E) Schematic view of the cross section of the device shows different heights of the cell chambers and migration channels.

device was used for observing non-SWCNT-exposed cells. Four reservoirs with a diameter of 6 mm were punched for cells, serum-free media, and FBS-containing media loading during the experiment, respectively. The cell-seeding/receiving chambers had a width of 600 μm and a height of 160 μm. The migration channels were 400 μm in length, 75 μm in width, and 16 μm in height. The aspect ratio of the migration channels was lower than that of the cell-seeding/receiving chambers, and thus the resistance of the migration channels was much higher to better control the chemical diffusion and gradient generation.

Standard photolithography was used for the master mold fabrication and polydimethylsiloxane (PDMS) soft lithography was used for the microfluidic gradient device fabrication. As shown in figure 1(A), the bottom layer of mold, which defined the molding areas for five migration channels and cell-seeding/receiving chambers, were fabricated by SU-8 2025. The thickness of this layer was referred to the information sheet from MicroChem and controlled by spinning the SU-8 at 4000 rpm for 60 s. After spun-coating, this layer was first soft baked at 65 °C (1 min) and 95 °C (5 min), then exposed under UV light, post-baked at 65 °C (1 min) and 95 °C (5 min), and finally developed and hard-baked at 150 °C for 1 h. The actual thickness of the fabricated layer was measured and confirmed as 16 μm using a profilometer (Tencor Alpha-Step 200). To fabricate the top molding layer (figure 1(B)),

which defined the molding areas for cell-seeding/receiving chambers on top of the bottom thin SU-8 layer, a high-viscous SU-8 2075 was spun-coated over the bottom layer at 1500 rpm for 30 s to generate a thicker top layer. This layer was then soft baked at 65 °C (7 min) and 95 °C (30 min). To align the bottom and top molding areas for cell-seeding/receiving chambers, alignment marks were designed and fabricated as shown in figure 1, and a mask aligner (Karl Suss MJB3) was used for pattern alignment. After UV exposure, the top layer SU-8 was post baked at 65 °C (5 min) and 95 °C (15 min), and developed. Finally, the mold was hard baked at 150 °C for 1 h and was ready for PDMS replication. The thickness of the cell-seeding and cell-receiving chambers was measured and confirmed as 160 μm by the profilometer. The mold was ready for the gradient device fabrication.

During PDMS soft lithography, silicone elastomer base (Slygard 184, Dow Chemical) was mixed with curing agent (Slygard 184, Dow Chemical) at a ratio of 10:1 and cast onto the master mold to obtain a 3 mm thick PDMS slab. PDMS was cured in an oven at 60 °C for 3 h, and then a thick PDMS slab was cut and peeled off from the mold. The reservoirs for cell and media loading were punched using a 6 mm diameter puncher. As shown in figure 1, two replicated PDMS devices and a glass slide were treated with oxygen plasma (50 W, 100 mTorr) for 20 s, and were brought together to form a permanent irreversible bonding. Before the cell experiment, the microfluidic devices were filled with deionized water and UV sterilized for 8 h in a biosafety hood.

2.2. Gradient characterization

In cell chemotaxis and migration studies, fluorescence molecules are commonly used to visualize a gradient for its characterization. The choice of fluorescence molecules is based on their molecular weights, which need to be similar or same as those of chemoattractants used for cell chemotaxis studies. In our experiment, fetal bovine serum (FBS) was used as the chemoattractant because it contains a mixture of natural chemokines and is widely used as the chemoattractant in migration assays. The majority component in FBS is bovine serum albumin, and thus albumin–fluorescein isothiocyanate conjugate (FITC-albumin) from albumin bovine was selected as the fluorescent marker. In addition, 10% FBS is commonly used to study mesothelial cells' migration in the Transwell assay, and we used 10% FITC-albumin as a representative concentration for monitoring gradient development and characterization.

A challenge for static gradient generation resides in maintaining a diffusion-dominant environment in the presence of pressure differences that can occur in experimental situations. Unwanted pressure differences generate convection and can prevent the setup of a stable gradient (Berthier *et al* 2010), To prevent pressure differences, the device shown in figure 1 was first loaded with M199 media, and then M199 media inside the reservoirs connecting cell-receiving chambers were carefully removed and refilled with the same volume of 10% FITC-albumin M199 media solution. The liquid levels in both reservoirs were kept at the same level with removing and refilling same volume of solutions, and then covered with thin PDMS layers, to prevent liquid evaporation. The liquid levels in two reservoirs on the cell-seeding side were also kept identicall and covered with thin PDMS layers during the operation. Additionally, sterilized wetted tissue was placed beside the device and enclosed together with the device in a petri dish using Parafilm® M film to further prevent liquid evaporation during 24 h imaging at 37 °C. Furthermore, the fluorescence live cell imaging microscope (Nikon Eclipse Ti, Japan) equipped the microscope cage incubator (OKOLab, Italy) is capable of precisely controlling temperature and humidity. The incubation cage was prewarmed for 1 h before loading the devices.

2.3. Simulation

A 3D numerical transient diffusion model was built and the simulation was conducted using commercial software COMSOL Multiphysics 5.0. The dimensions of the model were set the same as the actual fabricated device. The transport of the concentrated FBS was simulated using the transport of diluted species node. The governing equation is:

$$\frac{\partial c}{\partial t} + u \cdot \nabla c = \nabla \cdot (D \nabla c) + R$$

where c is the concentration of the species (mol m^{-3}), D is the diffusion coefficient of human serum albumin in water (6.1×10^{-11} m^2 s^{-1}) (BNID 100612) from (Milo *et al* 2010) because human serum albumin has the same molecular weight as the FBS, R is the reaction rate expression for the species (mol (m^3 s)$^{-1}$), and u is the velocity vector (m s^{-1}). To simulate the static gradient development, the governing equation was simplified as the diffusion-based form only, as:

$$\frac{\partial c}{\partial t} = \nabla \cdot (D \nabla c) + R$$

and a 'no flux' boundary condition was set on all the exterior boundaries.

2.4. Cell culture and chronic SWCNT exposure

Human pleural mesothelial (MeT5A) cells were acquired from the American Type Culture Collection (Manassas, VA) and maintained in M199 medium (Life Technologies, Grand Island, NY) supplemented with 5% FBS, 2 mM L-glutamine, 100 U mL^{-1} penicillin/streptomycin, 1 μg mL^{-1} epidermal growth factor (EGF) and 50 μg mL^{-1} hydrocortisone. Cell culture was performed in a humidified atmosphere of 5% CO_2 at 37 °C. SWCNTs, synthesized by high-pressure carbon monoxide disproportionate process (HiPCO), were obtained from Carbon Nanotechnology (CNI, Houston, TX). Elemental analysis of the supplied SWCNTs by nitric acid dissolution and inductively coupled plasma atomic emission spectrometry (ICP-AES; NMAM #7300) showed that the SWCNTs were 99% elemental carbon and contained less than 1% w/w of contaminants. Diameter and length distribution of dispersed SWCNT measured by field emission scanning electron microscopy (FESEM; model S-4800; Hitachi, Tokyo,

Japan) demonstrated 1.42 μm mean length and 0.38 μm mean width, respectively. Particles possessed surface areas between 400–1040 $m^2 g^{-1}$.

The cells were continuously exposed to a subcytotoxic surface area dose of 0.02 $\mu g\,cm^{-2}$ of SWCNTs for 4 months following the method previously described (Wang *et al* 2013). The determination of treatment dose was based on *in vivo* CNT exposure conditions with the reported total lung burden dose of 20 μg in mice (Porter *et al* 2010). The penetration of CNTs from the lung periphery into the pleural space after pulmonary exposure was quantified and 0.6% of the deposited CNT burden was found to reach the visceral pleura. From the estimated pleural surface area of 5 cm^2 in mice, the possible dose of CNT per square centimeter of visceral pleura is approximately 0.024 $\mu g\,cm^{-2}$. During the cell culture, 0.1 $mg\,mL^{-1}$ stocks of SWCNTs in phosphate buffer saline (PBS) containing 150 $\mu g\,mL^{-1}$ Survanta® (Abbott Laboratories, Abbott Park, IL) were sonicated and diluted in media (0.1 $\mu g\,mL^{-1}$) prior to cell exposure. Cells were exposed to the dispersed particles every 3 d following a PBS wash and passaged once per week to initial seeding densities.

2.5. Real-time imaging

A Nikon Eclipse Ti inverted fluorescence microscope (Nikon Japan) equipped with an OKOLab (Italy) Cage incubation system was used for the long-term and real-time imaging. The microscope was fully automated for imaging multiple positions in sequence, and equipped with long working distance objectives to rapidly acquire high-resolution phase contrast and fluorescent real-time images. The cage incubator system included an enclosure, a temperature-control module, CO_2 and humidity modules, and a stage insert chamber. For our experiment, three positions, including one at the cell-seeding chamber, one at the migration channel, and one at the cell-receiving chamber, were imaged and tracked for each migration channel, and a total of 15 positions were recorded for each device. At each position, bright field images were taken every 15 min over a period of 24 h.

2.6. Analysis of cell migration

Cell migration was analyzed when the stable gradient was established. ImageJ was used to track and analyze cell movement. Those MeT5A cells that migrated over a distance of two cell diameters (about 120 μm) from their original positions and kept moving along the gradient were counted as exhibiting responses to the FBS gradient. The cells that remained within a 120 μm radius of their original positions were excluded from the analysis, as were any cells that stopped or detached from the substrate. Cell morphological changes prior to/during/after their migrations were imaged and analyzed. Additionally, cell migration was characterized in terms of three parameters: speed of migration, direction of migration, and the number of cells migrating. The speed of migration was calculated as the distance of cell trajectory along the channel divided by cell migration time. The direction of migration can be either toward or away from the gradient. With an image-stitching technique supported by the Nikon NIS Element software, large images were taken before and after each experiment. The numbers of cells in the areas of interest in the corresponding large images were counted. Three experiments were performed for each test. The results were evaluated by *t*-test.

3. Results and discussion

3.1. Gradient development

The gradient was formed through the migration channels interconnecting the cell-seeding chambers and the cell-receiving chambers. Fluorescence images were taken every 15 min for 24 h using the inverted fluorescence microscope. The fluorescence intensities in the region of the migration channels were recorded as shown in figure 2(A) and were analyzed by ImageJ. Additionally, the 3D COMSOL simulation was performed to predict the gradient development along the migration channels as shown in supplemental figure 1 (stacks.iop.org/JMM/25/075010/mmedia).

In microfluidic systems it is difficult to match fluid levels precisely within input reservoirs, even though the media and solutions were carefully removed and refilled with the same volumes and PDMS films were used to cover the reservoirs to prevent evaporation effects on fluid flow. In order to limit fluid flow resulting from small pressure differences, the fabricated migration channels were shallow in height (16 μm) and narrow in width (75 μm), and the cell-seeding and receiving chambers were 10 times deeper in height (160 μm) and 3.5 cm in length between the reservoirs on each side. This design helped to create a high fluidic resistance within the migration channels to minimize the convective flow from the FBS loading site due to any pressure difference.

During the gradient characterization with FITC-albumin, upon introduction of the FITC-albumin into the two reservoirs connected to the cell-receiving chamber, approximately 5–6 h were required for the gradients to gradually generate through the migration channels, with an additional 3–4 h for the gradients to be stabilized and kept steady until the end of the experiment (24 h in total). From the cell responses, we noticed that the adhered cells underwent morphological changes and polarized from a flattened shape to an elongated, spindle shape in about 6 h, indicating that the cells sensed the gradient near the regions close to the migration channels and were in the process for migration. Figure 2(B) shows the gradient concentration profiles along the migration channels at 6, 10, 14, and 24 h, respectively, based on the experimental results and the simulation. The selected hours indicated the initial established gradient that the cells started to sense (6 h), the established steady gradient (10 h), the gradient kept steady (14 h), and the gradient at the end of the experiment (24 h). Figure 2(C) shows the gradient slope at different times during the gradient development. These results showed a long time required for gradients to be stably established. The gradients gradually increased to a level to which the cells were more sensitive. The slope of a chemoattractant gradient is thought to influence the migration rate of cells *in vivo*. In general, the experimental data was consistent with the simulation well

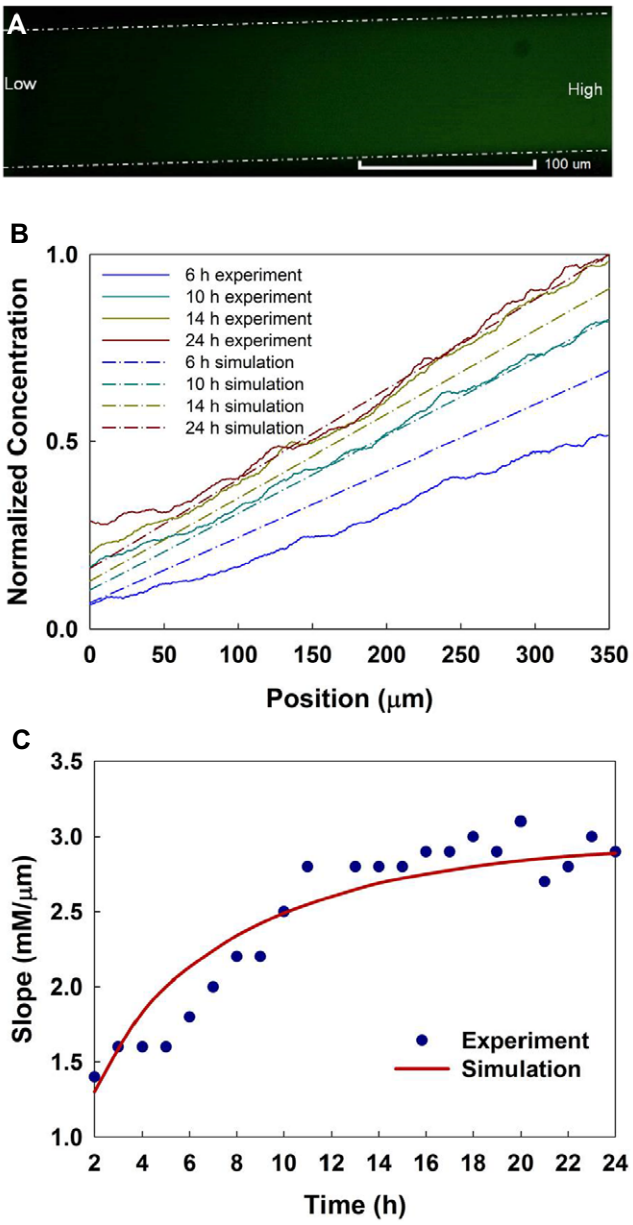

Figure 2. Characterization of the gradient development. (A) Fluorescence image shows the FITC-albumin gradient along a migration channel. Dashed white lines indicated the boundary of migration channel. Scale bar is 100 μm. (B) The normalized gradients along the migration channel at different time (6, 10, 14, and 24 h) were demonstrated based on the experimental results and the numerical simulation. (C) The characterization of the gradient slopes during the gradient development based on the experimental results and the numerical simulation.

for the gradient development as shown in the figures. At the steady state, a mass balance was reached within the system when the chemical flux entering the migrations channels equaled the chemical flux leaving the migration channels. Furthermore, each side chamber together with the reservoirs provided a much larger volume (172 μL) than the migration channels' volume (2.4 nL). Although the concentration near the regions of the migration channels in the cell-seeding chamber was not maintained at exactly zero, however, the small diffusing FBS flux from the migration channels was diluted by the large volume of FBS-free solution in the cell-seeding chamber. These factors helped to establish the steady-state gradient by not allowing the chemical species to accumulate in the chamber and reach a balanced state.

3.2. Cell morphology

After sterilization, two microfluidic devices were coated with 50 μg mL^{-1} fibronectin for 1 h at room temperature to enhance cell attachment. Then, the fibronectin solution was rinsed and replaced with serum-free M199 medium and the devices were kept inside an incubator to warm up. Subsequently, the chronically SWCNT-exposed MeT5A cells (1.5×10^6 cells per microliter) were loaded into the seeding chamber of one device, while the non-SWCNT-exposed MeT5A cells were loaded into the other device. Both devices were kept in the CO_2 incubator for 2 h until the cells start to attach. Finally, the devices were placed onto the microscope incubation stage for imaging.

Supplemental figure 2 (stacks.iop.org/JMM/25/075010/mmedia) illustrates the overall process of mesothelial cells migration inside the microfluidic gradient device. Initially after the cells were loaded inside the devices, it took about 2–3 h for the cells to adhere to the fibronectin-coated glass substrate. Most of the cells had a flattened shape after adhesion as shown in figures 3(A) and (E). Prior to migration, elongated, spindle shaped cells were clearly observed as shown in figures 3(B) and (F). The results indicated that the mesothelial cells underwent a morphological transition from a flattened shape to a spindle shape prior to migration. This morphological transition was gradually observed at approximately 6 h after the initial time point (figure 3(A) and supplemental movies S1 and S2). Additionally, the morphological transition observed in our experiment was similar to that of the mesothelial cells observed *in vivo* (Nagai *et al* 2013).

Although the numbers of cells at initial loading were controlled to be the same by keeping the same cell concentration and loading volume, the actual numbers of migrated cells were different when they moved into the channel. The migration channel was 75 μm in width, and as we observed in some situations, one cell or two cells migrated together through the channels along the bottom of the channels. During their subsequent migration, the cells kept their elongated shape and moved through the migration channel along the gradient direction (figures 3(C) and (G) and supplemental movies S3 and S4). In other situations, three or more cells migrated together through the channels during some part of their migration. In some of those cells, either the cells or parts of the cells adhered to the sidewalls and moved along the channels, and those cells normally showed considerably elongated shape during their migration. We also noticed that the majority of cells migrated in straight trajectories through the channels. After the cells migrated through the channels, they exhibited random movement with a flattened, less elongated shape in a uniform FBS concentration environment inside the cell-receiving chamber as shown in figures 3(D) and (H) and supplemental movies S5 and S6. Additionally, the

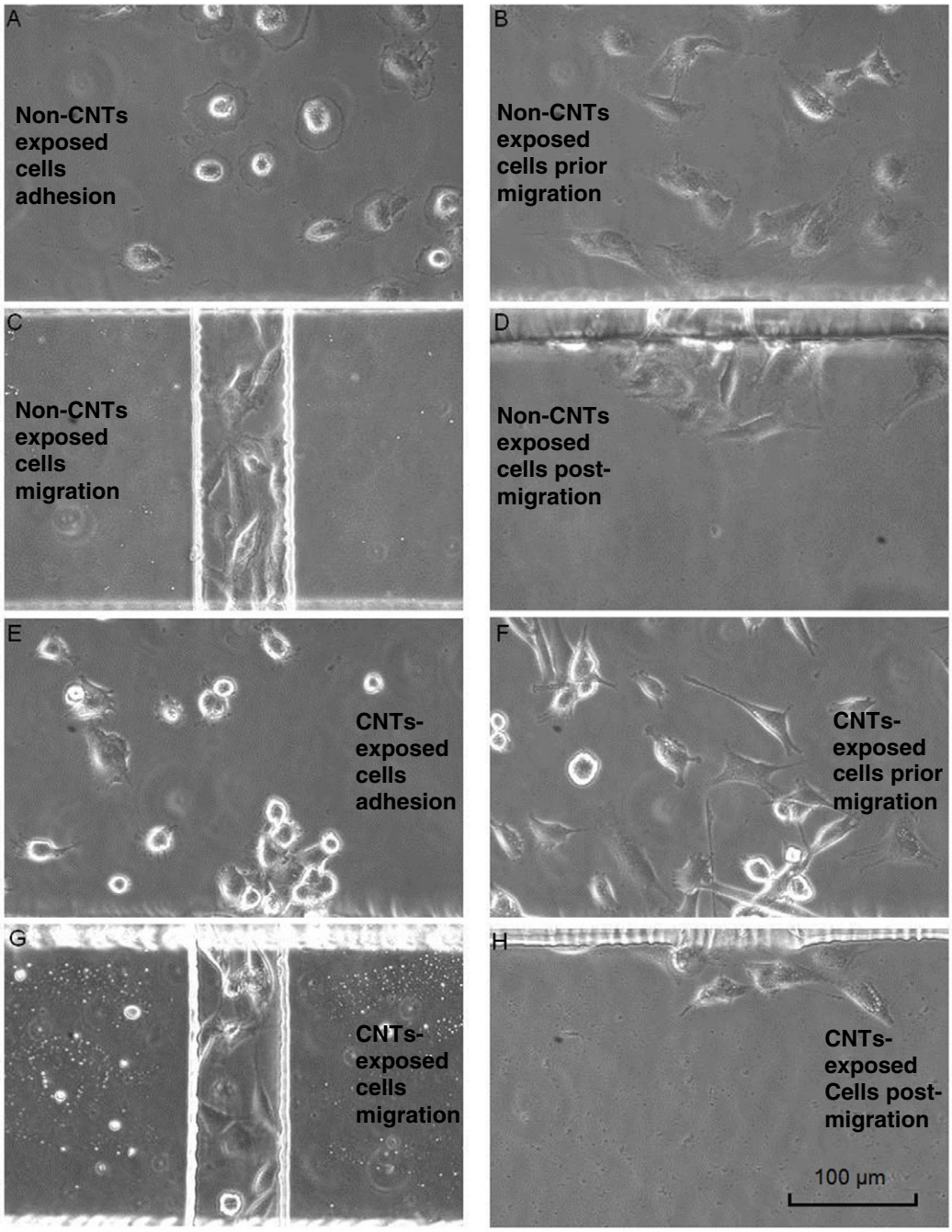

Figure 3. Cell morphologies shown at their adhesion, prior to migration, during migration and post migration, respectively. (A)–(D) show the morphology of non-SWCNT-exposed cells; (E)–(H) show the morphology of SWCNT-treated cells. Most of the cells were flattened after adhesion, and then gradually changed to spindle shapes prior to their migration. (A) Non-SWCNT exposed cells' morphology after the initial adhesion; (B) prior to their migration (~6 h after adhesion); (C) during their migration; (D) after their migration. (E) SWCNT-exposed cells' morphology after initial adhesion; (F) prior to their migration; (G) during their migration; (H) after their migration. Scale bar is 100 μm.

non-SWCNT-exposed and SWCNT-exposed cells exhibited similar migratory behavior and morphology.

It has been suggested that mesothelial cells need to undergo morphological transitions in response to inflammation and injury (Whitaker and Papadimitriou 1985, Fotev *et al* 1987). Because chronic injury and inflammation could trigger or promote tumor formation by sharing some common signaling mechanisms (Bjerkvig *et al* 2005), monitoring of morphological changes may provide a clue to malignant transformation. Most conventional assays described in the previous section do not detect morphological changes during cell migration. Our microfluidic gradient device provides the technique and experimental approach that allows direct observation of the cellular dynamics and morphological transitions during cell migration, which can be virtually applied to any cell types. The real-time monitoring feature of this system

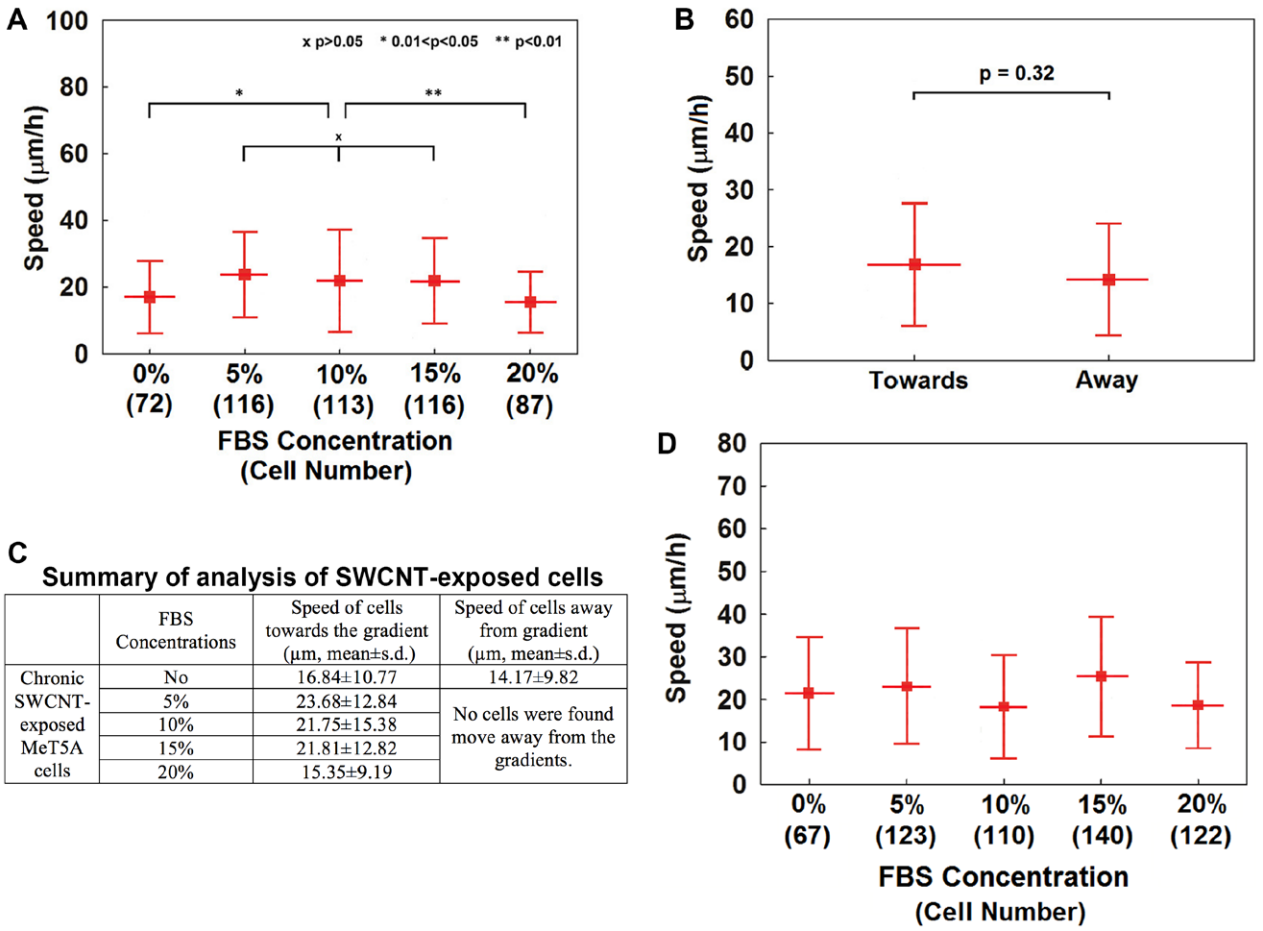

C

Summary of analysis of SWCNT-exposed cells

	FBS Concentrations	Speed of cells towards the gradient (μm, mean±s.d.)	Speed of cells away from gradient (μm, mean±s.d.)
Chronic SWCNT-exposed MeT5A cells	No	16.84±10.77	14.17±9.82
	5%	23.68±12.84	No cells were found move away from the gradients.
	10%	21.75±15.38	
	15%	21.81±12.82	
	20%	15.35±9.19	

Figure 4. Average migratory speeds for the tracked chronically SWCNT-exposed cells and non-SWCNT-exposed cells. (A) Average migration speeds for chronically SWCNT-exposed cells under different FBS concentration gradients. (B) Average migration speeds for chronically SWCNT-exposed cells under no FBS presence. The cells moved in both directions at comparable speeds. (C) Summary of analysis of the SWCNT-exposed cells. (D) Average migration speeds for non-SWCNT-exposed cells under different FBS concentration gradients. The experiments were performed three times for each situation. The error bars are standard deviations.

would be also useful for tracking interested molecules, e.g. genes and proteins, to study their role in the migratory process.

3.3. Migration under different FBS concentration gradients

Different concentrations of FBS ranging from 5 to 20% were used to compare the migratory activity of SWCNT-exposed and non-SWCNT exposed MeT5A cells. FBS was used as the chemoattractant because it contains a mixture of natural chemokines and is widely used as a chemoattractant in the Transwell migration assay (Breckenridge *et al* 2010). In general, the speeds observed in our experiment were consistent with those observed *in vivo* with the reported values of 6–24 $\mu m\,h^{-1}$ for mesothelial cells (Nagai *et al* 2013). As shown in figure 4(A), the average migratory speeds of SWCNT-exposed cells under different FBS concentration gradients were compared. The raw data of the speeds for individual tracked cells were provided in the supplementary information (supplemental figure 3) (stacks.iop.org/JMM/25/075010/mmedia). The cells moved significantly faster under 5% ($23.68 \pm 12.84\,\mu m\,h^{-1}$, $p < 0.01$), 10% ($21.75 \pm 15.38\,\mu m\,h^{-1}$, $p < 0.01$), and 15% ($21.81 \pm 12.82\,\mu m\,h^{-1}$, $p < 0.01$) FBS concentration gradients compared to the speed with no FBS ($16.84 \pm 10.77\,\mu m\,h^{-1}$). A significantly slower movement of SWCNT-exposed cells ($15.35 \pm 9.19\,\mu m\,h^{-1}$, $p < 0.001$) was observed under the 20% FBS concentration gradient compared to other concentration gradients. Additionally, when there was no FBS present, the cells showed random movement in the connection region of the cell-seeding chamber and the migration channel (supplemental movie S7). In the migration channels, the cells were observed moving toward the cell-receiving chambers; however, a comparable number of cells was observed to move in the opposite direction, away from the cell-receiving chamber. As shown in figure 4(B), those cells showed similar migration speeds (toward: $16.84 \pm 10.77\,\mu m\,h^{-1}$; away: $14.17 \pm 9.82\,\mu m\,h^{-1}$; $p = 0.32$). No cells were observed moving against the gradient direction when a FBS gradient was present. From these results, the SWCNT-exposed cells demonstrated their increasing migration activities from low FBS concentration gradient to higher concentration gradient compared to the non-SWCNT-exposed cells group, in which the speeds for cell migration towards the gradients were varied (figure 4(D)), cells migration against the gradient was always observed, and no clear migration patterns or trends for non-SWCNT-exposed cells

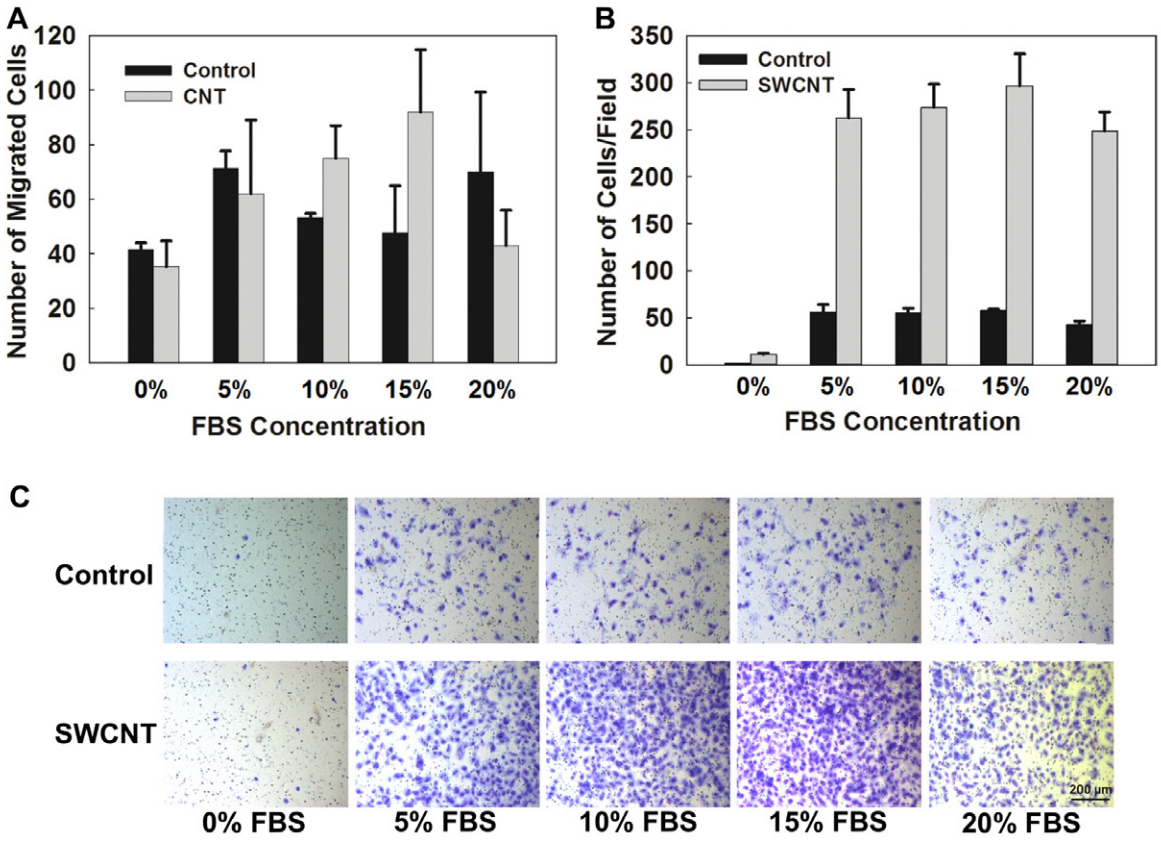

Figure 5. (A) Average number of migrating cells observed inside microfluidic gradient devices under different FBS concentration gradients for chronically SWCNT-exposed cells and non-SWCNT-exposed cells (control). (B) Average number of migrating cells observed inside the Transwell assays under different FBS concentration gradients for chronically SWCNT-exposed cells and non-SWCNT-exposed cells (control). (C) Representative images showing the cells migrated through the Transwell insert membrane under different FBS concentrations. The experiments were performed three times for each condition. Values are represented as the mean ± s.e.m.

were able to be tracked under the conditions with or without the presence of FBS chemical gradients.

3.4. Number of migrated cells

The number of migrated cells is a parameter commonly used in conventional Transwell migration assay to indicate and characterize cell migration. Cell migration with increasing numbers is traditionally considered as a cancer hallmark and a key characteristic of aggressive tumors. Additionally, it can be used as a predictive indicator for metastasis.

For this study using the microfluidic gradient device, the number of migrated cells was counted based on the method introduced in the 'Materials and methods' section. Data for the number of migrating cells were extracted and compared for each FBS concentration as shown in figure 5(A). Additionally, we performed parallel experiments using the Transwell assay under different FBS concentrations as shown in figure 5(B). Compared to the no-FBS condition, an increased number of migrating cells in the presence of FBS was observed from SWCNT-exposed and non-SWCNT exposed cells in both microfluidic and Transwell assays. For SWCNT-exposed cells, the number of migrating cells increased with increasing FBS concentration gradients from no FBS presented to 15% FBS, which were shown as 35 cells at no FBS presence, 62 cells at 5% FBS, 75 cells at 10% FBS, and 92 cells at 15% FBS respectively for an average number from three experiments for each condition.

For the 20% FBS concentration gradient, dramatically decreased number of SWCNT-exposed cells (43 cells at 20% FBS) was observed in the cell-receiving chamber within the same experimental duration. The same trend of responses for SWCNT-exposed cells was also observed in the Transwell assay (figures 5(B) and (C)) with a reduced number of migrated cells under the 20% FBS concentration. The possible reason can be explained from the microfluidic experiment based on the migration speeds of these cells shown in figure 4. The exposed cells were able to respond to the presence of the FBS gradient; however, they demonstrated significantly reduced migration speeds, which then resulted in the reduced number of migrated cells.

For non-SWCNT-exposed cells, no clearly increasing trajectory for the number of migrating cells was observed under different FBS concentrations in the Transwell assay. Similar findings were observed in microfluidic studies in which the number of migrated cells was varied under each condition and no clear pattern was able to track. From this study, the chronically SWCNT-exposed mesothelial cells demonstrated more sensitive towards the gradient changes compared to the non-SWCNT-exposed cells.

Additionally, because the experiments were performed and imaged over 24 h, the cells' divisions were observed during the experiments. In our previous reported work using Transwell assay (Lohcharoenkal *et al* 2013), Cyquant cell proliferation and Hoechst 33342 assays were used to evaluate the exposed cells' growth characteristics. The results showed that chronically SWCNT-exposed mesothelial cells induced cell growth about 1.5 times higher than that of non-SWCNT-exposed cells. In the microfluidic experiments, we observed more cell divisions in SWCNT-treated cells. Figure 5 actually reflected the final result due to two effects: cell migration by sensing the gradients and cell proliferation. However, for the studies of migration speeds in figure 4, the images were taken with a 15 min interval, and cell divisions were caught in some images, but it was not possible to capture all cell divisions through the whole experimental duration. In our future studies, it will be necessary to combine proliferation assay analysis with cell migration studies.

3.5. Biological mesothelial cell model for assessment of nanotoxicity

With similar fibrous morphology and mode of exposure to asbestos, growing concerns have arisen for elevated risk of CNT-induced lung carcinogenesis. Evidence has shown that CNTs are biopersistent and can cause lung damage (Shvedova *et al* 2005, Mercer *et al* 2008); however, relatively little is known about the long-term carcinogenic effects of CNTs. We have previously shown the malignant transformation of these CNT-exposed cells. Transwell assays were used for the studies of cell migration in these experiments, and cell migration with increased numbers was considered as one of the major features indicating neoplasticlike transformation phenotype and the aggressiveness of these mesothelial cells upon CNT exposure (Lohcharoenkal *et al* 2013, Wang *et al* 2013).

The assessment of cell models for gradient sensing is closely tied to technological advances (Berthier and Beebe 2014). 1- and 2D static microfluidic gradient devices with a similar gradient generation approach have been applied for studies of cell chemotaxis responses, and human neutrophils or neutrophil-like cells, as very useful human cell migration models, were studied most in publications (Berthier *et al* 2010, Butler *et al* 2010, Boneschansker *et al* 2014). Compared with neutrophils, mesothelial cells are less studied in their sensing of gradients. However, the chronically CNT-exposed mesothelial cell is considered as a biological cell model for predicting mesothelioma pathogenicity of nanomaterials and assisting mechanistic studies of the cellular and molecular events leading to mesothelioma. There is a vital need to develop more physiologically relevant cell models for better assessment and characterization of the mesothelioma hazard posed by nanomaterials, and technologies like microscale platforms to control spatiotemporal chemical gradients in a reliable and precise way.

From our studies, the challenges of studying mesothelial cells' migration using microfluidic gradient devices are: 1) they are adherent cells and require an appropriate molecular coating and coating concentrations as well as considerable cell seeding time. We tested collagen and fibronectin coatings with varied concentrations and found 50 μg mL^{-1} fibronectin coating provided the best results for cell adhesion and mesothelial cells migration in sensing the gradients. 2) Shear stress greatly affects mesothelial cells' adhesion and survival. In our early experiments using laminar flow-based microfluidic gradient device, the gradients were generated and maintained because of the continuous flows from differently concentrated streams, the cells continuously exposed under the shear stress and gradually showed loss of their attachment on the substrate, and then died during the experiment without apparent migration under the gradients. 3) The mesothelial cells demonstrated slow migration speeds and it is critical to controll the gradient in a reliable and precise way. Laminar flow-based gradient devices are not suitable for studies of mesothelial cells because of continuous shear stress exposure on cells, as shown in our previous attempts. Thus, a better option for cell migration would be static gradient devices similar to our design, in which the passive diffusion of FBS from the reservoirs into the cell-receiving chamber created a gradient in which the highest concentrations were in the cell-receiving chamber and the lowest concentrations were in the regions of the migration channels connected to the cell-seeding chamber. 4) Controlling the gradient regions. Different to the Transwell assay, the cell seeding densities were harder to be controlled in microfluidic gradient devices. The cells in the regions close to the migration channels can sense the gradient quickly and migrate through the migration channels. Cells beyond these regions might sense the gradient and migrate toward the channels; however, these cells have less chance of entering the channel due to their migration speeds (based on the measured speeds) and the experimental duration. The static gradient device needs better optimization of the design to control the cell population exposed under the gradient environment and have majority cells sensing the gradients as well as keeping a long-term stable gradient.

4. Conclusions

We presented a microfluidic static gradient device for studying cell migration and the effect of chronic SWCNT exposure on mesothelial cell migration. The device presented here demonstrated a reliable approach to generate gradients under diffusion while effectively reducing convective flow. The device allows real-time tracking and identification of cell migration at a single-cell level. More migration signatures related to chronic CNT exposure of mesothelial cells could be investigated using the microfluidic gradient device at first time, and this provides benefits over the conventional Transwell assay, in which the cell migration number is the only parameter to be tracked. Using this method, we demonstrated that chronic exposure to SWCNTs increased the migratory activity of human pleural mesothelial cells compared to non-SWCNT-exposed cells, supporting their mesothelioma pathogenicity.

This platform would be much needed for supporting the development of more physiologically relevant cell models for better assessments and characterization of mesothelioma hazard of nanomaterials. Furthermore, the knowledge obtained from this study would be valuable for the development of 3D cell migration or cell invasive models in future studies of malignant mesothelial cells. The described microfluidic gradient device could be used to study the migration of other cell types in which a gradient generated by non-shear flow conditions may be more preferable.

Acknowledgments

This work was supported by the National Science Foundation (NSF-1227359, NSF-1336205) and by WV EPSCoR program (EPS-1003907) funded by the National Science Foundation. The microfabrication work was performed in Shared Research Facilities (Cleanroom facilities) and Microfluidic Integrative Cellular Research on Chip Laboratory (MICRoChip Lab) at West Virginia University.

References

Berthier E and Beebe D J 2014 Gradient generation platforms: new directions for an established microfluidic technology *Lab Chip* **14** 3241–7

Berthier E, Surfus J, Verbsky J, Huttenlocher A and Beebe D 2010 An arrayed high-content chemotaxis assay for patient diagnosis *Integr. Biol.* **2** 630–8

Bjerkvig R, Tysnes B B, Aboody K S, Najbauer J and Terzis A J 2005 Opinion: the origin of the cancer stem cell: current controversies and new insights *Nat. Rev. Cancer* **5** 899–904

Boneschansker L, Yan J, Wong E, Briscoe D M and Irimia D 2014 Microfluidic platform for the quantitative analysis of leukocyte migration signatures *Nat. Commun.* **5** 4787

Boyden S 1962 The chemotactic effect of mixtures of antibody and antigen on polymorphonuclear leucocytes *J. Exp. Med.* **115** 453–66

Breckenridge M, Egelhoff T and Baskaran H 2010 A microfluidic imaging chamber for the direct observation of chemotactic transmigration *Biomed. Microdevices* **12** 543–53

Bridda A, Padoan I, Mencarelli R and Frego M 2007 Peritoneal mesothelioma: a review *MedGenMed* **9** 32

Butler K L, Ambravaneswaran V, Agrawal N, Bilodeau M, Toner M, Tompkins R G, Fagan S and Irimia D 2010 Burn injury reduces neutrophil directional migration speed in microfluidic devices *PLoS One* **5** e11921

Carbone M, Kratzke R A and Testa J R 2002 The pathogenesis of mesothelioma *Semin. Oncol.* **29** 2–17

Cho S Y and Klemke R L 2000 Extracellular-regulated kinase activation and CAS/Crk coupling regulate cell migration and suppress apoptosis during invasion of the extracellular matrix *J. Cell Biol.* **149** 223–36

Chou C-C, Hsiao H-Y, Hong Q-S, Chen C-H, Peng Y-W, Chen H-W and Yang P-C 2008 Single-walled carbon nanotubes can induce pulmonary injury in mouse model *Nano Lett.* **8** 437–45

Diao J, Young L, Kim S, Fogarty E A, Heilman S M, Zhou P, Shuler M L, Wu M and DeLisa M P 2006 A three-channel microfluidic device for generating static linear gradients and its application to the quantitative analysis of bacterial chemotaxis *Lab Chip* **6** 381–8

Elgrabli D, Floriani M, Abella-Gallart S, Meunier L, Gamez C, Delalain P, Rogerieux F, Boczkowski J and Lacroix G 2008 Biodistribution and clearance of instilled carbon nanotubes in rat lung *Part. Fibre Toxicol.* **5** 20

Foldvari M and Bagonluri M 2008 Carbon nanotubes as functional excipients for nanomedicines: I. Pharmaceutical properties *Nanomed.: Nanotechnol. Biol. Med.* **4** 173–82

Fotev Z, Whitaker D and Papadimitriou J M 1987 Role of macrophages in mesothelial healing *J. Pathol.* **151** 209–19

Frevert C W, Boggy G, Keenan T M and Folch A 2006 Measurement of cell migration in response to an evolving radial chemokine gradient triggered by a microvalve *Lab Chip* **6** 849–56

Heit B and Kubes P 2003 Measuring chemotaxis and chemokinesis: the under-agarose cell migration assay *Sci. STKE* **2003** PL5

Irimia D 2014 Cell migration in confined environments *Methods in Cell Biology* vol 121 ed P Matthieu and T Manuel (San Diego, CA: Academic) pp 141–53

Kaufman A and Flores R 2011 Surgical treatment of malignant pleural mesothelioma *Curr. Treat. Options Oncol.* **12** 201–16

Kim S, H J Kim and N L Jeon 2010 Biological applications of microfluidic gradient devices. *Integr. Biol.* **2** 584–603

Lam C W, James J T, McCluskey R and Hunter R L 2004 Pulmonary toxicity of single-wall carbon nanotubes in mice 7 and 90 d after intratracheal instillation *Toxicol. Sci.* **77** 126–34

Liu Y, Sai J, Richmond A and Wikswo J P 2008 Microfluidic switching system for analyzing chemotaxis responses of wortmannin-inhibited HL-60 cells *Biomed. Microdevices* **10** 499–507

Lohcharoenkal W, Wang L, Stueckle T A, Dinu C Z, Castranova V, Liu Y and Rojanasakul Y 2013 Chronic exposure to carbon nanotubes induces invasion of human mesothelial cells through matrix metalloproteinase-2 *ACS Nano* **7** 7711–23

Martin J, Yung S, Robson R L, Steadman R and Davies M 2000 Production and regulation of matrix metalloproteinases and their inhibitors by human peritoneal mesothelial cells *Perit. Dial. Int.* **20** 524–33

Mercer R R, Hubbs A F, Scabilloni J F, Wang L, Battelli L A, Friend S, Castranova V and Porter D W 2011 Pulmonary fibrotic response to aspiration of multi-walled carbon nanotubes *Part. Fibre Toxicol.* **8** 21

Mercer R R, Scabilloni J, Wang L, Kisin E, Murray A R, Schwegler-Berry D, Shvedova A A and Castranova V 2008 Alteration of deposition pattern and pulmonary response as a result of improved dispersion of aspirated single-walled carbon nanotubes in a mouse model *Am. J. Physiol. Lung Cell. Mol. Physiol.* **294** L87–97

Milo R, Jorgensen P, Moran U, Weber G and Springer M 2010 BioNumbers—the database of key numbers in molecular and cell biology *Nucl. Acids Res.* **38**(suppl 1) D750–3

Muller J, Huaux F, Moreau N, Misson P, Heilier J-F, Delos M, Arras M, Fonseca A, Nagy J B and Lison D 2005 Respiratory toxicity of multi-wall carbon nanotubes *Toxicol. Appl. Pharmacol.* **207** 221–31

Mutsaers S E 2002 Mesothelial cells: their structure, function and role in serosal repair *Respirology* **7** 171–91

Nagai H, Chew S H, Okazaki Y, Funahashi S, Namba T, Kato T, Enomoto A, Jiang L, Akatsuka S and Toyokuni S 2013 Metamorphosis of mesothelial cells with active horizontal motility in tissue culture *Sci. Rep.* **3** 1144

Porter D W *et al* 2010 Mouse pulmonary dose- and time course-responses induced by exposure to multi-walled carbon nanotubes *Toxicology* **269** 136–47

Servant G, Weiner O D, Neptune E R, Sedat J W and Bourne H R 1999 Dynamics of a chemoattractant receptor in living neutrophils during chemotaxis *Mol. Biol. Cell* **10** 1163–78

Shvedova A A, Kisin E R, Porter D, Schulte P, Kagan V E, Fadeel B and Castranova V 2009 Mechanisms of pulmonary toxicity and medical applications of carbon nanotubes: two faces of Janus? *Pharmacol. Ther.* **121** 192–204

Shvedova A A *et al* 2005 Unusual inflammatory and fibrogenic pulmonary responses to single-walled carbon nanotubes in mice *Am. J. Physiol. Lung Cell. Mol. Physiol.* **289** L698–708

Valle M T, Degl'Innocenti M L, Bertelli R, Facchetti P, Perfumo F, Fenoglio D, Kunkl A, Gusmano R and Manca F 1995 Antigen-presenting function of human peritoneum mesothelial cells *Clin. Exp. Immunol.* **101** 172–6

von der Mark K, Schöber S and Goodman S 1999 Integrins in cell migration *Integrin Protocols* vol 129 ed A Howlett (Totowa, NJ: Humana Press) pp 219–30

Wang L, Castranova V, Mishra A, Chen B, Mercer R R, Schwegler-Berry D and Rojanasakul Y 2010 Dispersion of single-walled carbon nanotubes by a natural lung surfactant for pulmonary *in vitro* and *in vivo* toxicity studies *Part. Fibre Toxicol.* **7** 31

Wang L, Stueckle T A, Mishra A, Derk R, Meighan T, Castranova V and Rojanasakul Y 2013 Neoplastic-like transformation effect of single-walled and multi-walled carbon nanotubes compared to asbestos on human lung small airway epithelial cells *Nanotoxicology* **8** 485–507

Whitaker D and Papadimitriou J 1985 Mesothelial healing: morphological and kinetic investigations *J Pathol.* **145** 159–75

Zicha D, Dunn G A and Brown A F 1991 A new direct-viewing chemotaxis chamber *J. Cell Sci.* **99**(Pt 4) 769–75

Zigmond S H 1977 Ability of polymorphonuclear leukocytes to orient in gradients of chemotactic factors *J. Cell Biol.* **75**(2 Pt 1) 606–16